Probing Biomolecular Interactions Using Nanopore Force Spectroscopy

Olga K. Dudko
University of California, San Diego, La Jolla, CA, USA

Amit Meller
Boston University, Boston, MA, USA

The ability to apply a force on individual biomolecular complexes and measure their time-dependent response have begun to reveal their mechanical properties, interactions with other biomolecules, and self-interactions. A number of single-molecule methods have been developed and applied in the past decade to broad range of biological system, including proteins in the skeletal and cardiac muscle sarcomere, nucleic acid complexes, and enzymes. Nanopore force spectroscopy (NFS) is an emerging single-molecule method that takes advantage of the native electrical charge of biomolecule to exert a localized bond-rupture force. This article reviews the basic principles of the method and discusses two bond-breakage modes utilizing either a constant voltage or a fixed voltage ramp, which are related quantitatively in an essentially model-free way. A unified theoretical formalism is developed to extract kinetic information from the NFS data. The utility of this formalism is illustrated by analyzing data from nanopore unzipping of individual DNA hairpin molecules.

Encyclopedia of Analytical Chemistry R.A. Meyers (Ed.)
Copyright © 2009 John Wiley & Sons Ltd

1 INTRODUCTION

In living cells, mechanical forces are involved in many biological processes at the molecular level, and many biological macromolecules have load-bearing functions. Proteins such as titin in the skeletal and cardiac muscle sarcomere, fibronectin in the extracellular matrix, and spectrin in erythrocytes provide resistance under mechanical stress. Other biomolecules, such as higher-order nucleic acid complexes, are unraveled in a controlled way by mechanical forces when being processed by polymerases, helicases, and ribosomes. Remarkable advances in single-molecule manipulation have made it possible to measure the forces and strains that develop during these processes in real time. Moreover, the exertion of external forces modifies these processes in a *controlled* way, providing a powerful tool to study their structure, dynamics, and function.

The response of biomolecules to applied force can reveal mechanical properties, interactions with other biomolecules or self-interactions, and in some cases, structure. Single-molecule techniques like atomic force microscope (AFM) and optical or magnetic tweezers are the most direct methods of exerting and measuring forces on biomolecules, and thus have been applied to a broad variety of biological systems, ranging from nucleic acids to enzymes to motor proteins.[1–10] In these techniques, force is related to the displacement Δx of a bead or a cantilever, which is physically attached to the molecule, via Hooke's law ($F = -k\Delta x$), where k is the linear spring constant of the pulling apparatus. Nanopores, however, represent a fundamentally different approach for obtaining force spectroscopy data.[11] This emerging single-molecule technique utilizes native molecular electric charge to exert force on virtually any biomolecule when it is threaded through a single-nanoscale constriction.[12–16] In contrast to optical tweezers and AFM techniques, where force is applied mechanically to one point on the biomolecule by conjugation to a bead or cantilever, the force exerted on biomolecules using nanopore methods is both local to the region inside the pore and applied according to the molecule's charge in that region (Q_{eff}). Thus, this force is directly proportional to the electrical voltage drop across the pore (ΔV), $F = \frac{Q_{\text{eff}}}{l}\Delta V$, where l is the pore length, in an analogy to the Hookian relationship mentioned above. To quantify this force, the system's effective charge per unit length ($q_{\text{eff}} = Q_{\text{eff}}/l$) must be

determined under the conditions used in each specific experiment. The pore constriction itself then exerts a negative and equal force ($-q_{\text{eff}}\Delta V$) on the molecule. The mechanical force appears as a localized shear force that destabilizes any biomolecular bonds or structures that will not pass easily through the pore and can lead to their subsequent rupture.

Nanopore Force Spectroscopy (NFS) harnesses the functionality of nanopores in conjunction with controlled local application of forces at the single-molecule level for analytical purposes. This article focuses on the principles and applications of NFS in single-molecule studies. The two main approaches to force spectroscopy using nanopores involve applying a destabilizing force to a molecular bond either at a fixed force level or at a constantly increasing force level, to create mechanical tension. Eventually, the application of force will culminate in a molecular transition such as ligand–receptor dissociation, unfolding of a protein, or unzipping of nucleic acids. When performed at constant force (a constant voltage), these experiments directly probe the voltage-dependent lifetime of the system, $\tau(V)$. In contrast, the distribution of rupture voltages, $p(V)$ measured in experiments at a constant voltage-ramp speed needs to be processed to provide information about $\tau(V)$. This article discusses these two bond-breakage modes in the context of nanopore experiments and shows that the experimental outputs of these two modes are related quantitatively in an essentially model-free way. A unified theoretical formalism is developed to extract kinetic information from NFS data. The utility of this formalism is illustrated by analyzing data from nanopore unzipping of individual DNA hairpin molecules.

2 NANOPORE FORCE SPECTROSCOPY

2.1 Experimental Methods

In a nanopore experiment, an electrical force is applied directly to a charged biopolymer threaded through a narrow constriction of molecular size (a few nanometers), in an insulating thin membrane (Figure 1) separating two reservoirs of buffered salt solution (typically 0.1 M – 1 M of monovalent salt).[11] The electric field applied across two electrodes placed on either side of the membrane results in a steady ionic current through the pore (Figure 1(a)). Because the resistivity of the pore is orders of magnitude larger than the resistivity of the bulk solution, most of the electric field is localized to the pore region. Thus, the force applied on a threaded biopolymer is, to a good approximation, restricted to those parts residing in the pore. Unstructured single-stranded nucleic-acid polymers slide continuously through the pore – a process usually referred to as "*translocation*".[17] However, if the biopolymer's cross-section is not uniform, because of, for example, hairpin or bound proteins, so that a local cross-section is larger than the pore diameter, the translocation process will be suspended until this "obstacle" is cleared. Formally, the removal of these obstacles (i.e. unzipping of the hairpin, structures or stripping-off of bound proteins)

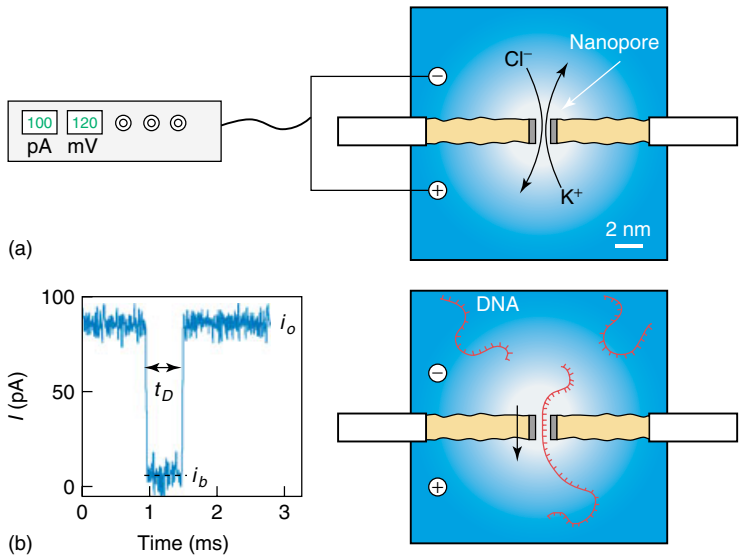

Figure 1 The nanopore method: (a) The ion current flowing through a single-nanoscale pore is measured using a pico-ampere electrometer. (b) The insertion and threading of biopolymers cause abrupt blockades in the ion current, during the time in which the molecules remain in the pore. An electrical field applied across the membrane results in a strong force, driving the charged biopolymers from the negative to the positive chambers.

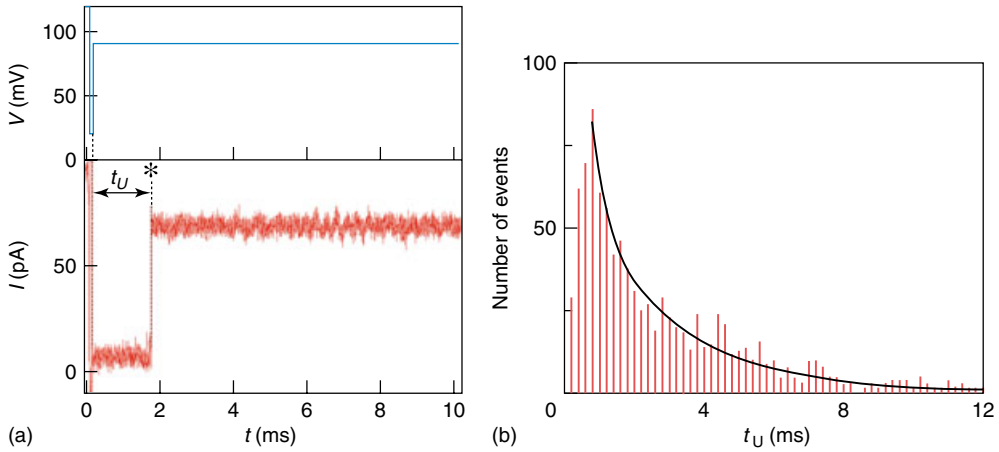

Figure 2 Bond rupture using a step in the applied voltage (or the force), when a molecule is threaded through the pore. (a) Top panel represent the applied voltage wave in each and every event. An abrupt drop in the measured ion current (lower panel) triggers the voltage wave generation. After the molecule is threaded inside the pore, the voltage is raised to a fixed level (90 mV in this case) and the current is monitored until an upward transition, signaling the bond rupture, is observed. The delay time from the moment that the step is applied to the rupture time (marked with a star) is the unzipping time, t_U. (b) A distribution of t_U measured for >1000 events as shown on the left. The distribution display a clear peak at ~1 ms and a decaying exponential tail with average time ~2.7 ms (solid line).

is described by a crossing of an energy barrier, in particular, an energy barrier that is much larger than that associated with moving an *unstructured* biopolymer through the pore. Because the waiting time associated with an energy-barrier crossing increases exponentially with the barrier height, the characteristic translocation times of unstructured biopolymers (i.e. single-strand (ss) DNA, ssRNA, or polypeptides) are a couple of orders of magnitude smaller than the typical time required to unzip, for example, a similar length hairpin.

Generally, the distinction is between two different kinds of bond-rupture measurements – pulling at a constant force or with a linearly increasing force (i.e. with a constant force ramp). In nanopore experiments, these two types of measurements can both be realized by dynamically modifying the voltage applied to the biomolecule after it has been threaded to the pore, using a computerized system.[18] The current flowing through the pore is constantly measured, and the computerized data-acquizition system is programmed to generate an output voltage signal triggered by an abrupt decrease in the pore current. Figure 2 illustrates one example of such an experiment, where a step in the voltage is applied after capture. The left panel (a) displays the applied voltage (top) and the pore current (bottom) measured during a typical unzipping event of a 10 bp DNA hairpin. The entry of the biomolecule to the pore creates an abrupt decrease in ion current, lowering it from the open pore- to the blocked-pore level, which triggers the dynamic voltage control system. After a brief period (sufficient for threading the molecule up to the hairpin), the voltage is set to a fixed level, V (90 mV in this case). Bond rupture (designated with an asterisk) is signaled by the jump in the ion current at $t = t_U$. Thousands of individual unzipping events like the one shown can be collected in couple of minutes, and a distribution of unzipping times can be constructed.[19] Panel (b) displays an unzipping time distribution for the 10 bp hairpin at a step of 90 mV, showing a peak at ~1 ms and an exponentially decaying tail with characteristic timescale ~2.7 ms (solid line). In a typical experiment, the dependence of τ_U on V is measured over a broad range of voltages. This method takes advantage of the fact that the translocation time of an unstructured (i.e. single stranded) DNA through the pore is couple of orders of magnitude faster (~2 μs per nucleotide)[14,15] than the unzipping time.[19] Thus, when threading a biopolymer through a pore, a short "threading" pulse is sufficient to ensure that the single-stranded portion of the molecule is fully threaded. Yet, the probability of unzipping hairpins with these short pulses is negligible.

Figure 3 displays a bond-rupture event using the *force ramp* method. In principle, dynamic voltage control can be used to apply any voltage waveform $V(t)$ to the biomolecule. The simplest waveform is a linearly increasing voltage (a constant loading rate). The top panel in Figure 3(a) displays the time-dependent voltage (top) triggered, as before, by the entry of the ssDNA overhang into the pore. Initially, the nanopore current (bottom) remains at the blocked level, but at roughly $t \sim 10$ ms, the hairpin is unzipped resulting in an abrupt jump (marked with an asterisk) in current to the open pore current level. The voltage at which bonds are ruptured is defined as V_U. Figure 3(b) displays a typical

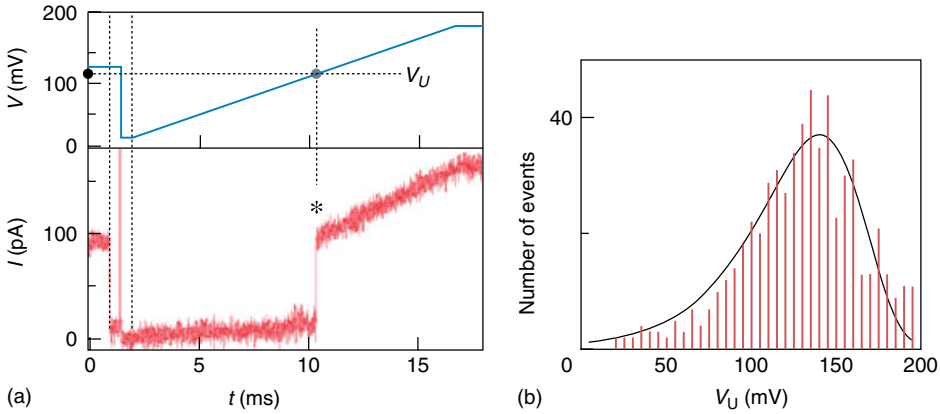

Figure 3 DNA unzipping event using a voltage ramp. (a) Top panel represent the applied voltage wave, and the bottom panel displays the measured pore current. The generation of the voltage wave is triggered by an abrupt drop in the ion current, which signals the entry of the DNA to the pore. After the molecule is threaded inside the pore, the voltage is raised at a fixed slope and the current is monitored until an upward transition (star), signaling the bond rapture, is observed. The voltage at which rupture occurs is defined as the unzipping voltage, V_U. (b) Distribution of >1000 unzipping events such as the one shown in (a), displaying one main peak at ~140 mV.

distribution of the rupture voltages for ~1000 individual unzipping events such as the one shown in Figure 3(a). In a typical experiment, distributions of unzipping events are collected for different loading rates.

In principle the two bond-rupture methods formally report the same information on the system, but there are practical differences between the two. For example, bond breakage at the limit of small, constant forces could be extremely time consuming and therefore often unpractical. However, the same regime of bond rupture can be effectively explored using force ramps because of the growing nature of the force. The unification of the two methods on a single ''master curve'', discussed below, reinforces this point.

2.2 Theory: From Phenomenological Approach to Unified Microscopic Description of Voltage-driven Molecular Rupture

With the spectacular resolution of forces and distances, NFS experiments have the potential to provide unprecedented insights into structure, dynamics, interactions, and mechanical properties of individual biomolecules. However, the interpretation of the experimental outputs in terms of underlying molecular interactions and structures often turns out to be an extremely challenging task, because these experiments are often carried out under nonequilibrium conditions. Moreover, the analysis of data obtained at the single-molecule level requires reformulation of many of the traditional concepts of thermodynamics and kinetics. To extract novel and reliable information from single-molecule force spectroscopy data, a solid theoretical basis has to be developed and linked to the experimental observables, such as the voltage-dependent lifetime of the system, $\tau(V)$, and the distribution of rupture forces, $p(V)$.

2.2.1 *Voltage-driven Molecular Bond Rupture as a Problem of Escape Over a Barrier*

In the following theoretical treatment, voltage-driven bond rupture in the nanopore is viewed as a force-induced quasi-irreversible molecular transition that connects two states separated by a barrier on a one-dimensional free-energy surface of the general shape drawn in Figure 4 along the reaction coordinate x. In the context of unzipping a DNA hairpin, the well of the free-energy surface represents the initial state, where the single-stranded overhang of DNA is threaded into the pore with the hairpin closed. Moving over the barrier into the ruptured state requires unzipping the double-stranded part of the DNA, so that the pore can be cleared, as illustrated in the cartoons in Figure 4(a). In the case of a molecular complex, such as that formed by DNA-protein interaction, the well of the free-energy surface represents the bound state, and crossing the barrier corresponds to dissociation.

In the absence of an applied voltage, the bare free-energy surface $G_0(x)$ is assumed to have a barrier at a distance $x^{\ddagger}$ from the well center and an activation-free energy $\Delta G^{\ddagger}$ (Figure 4a). The parameter $V^{\ddagger}$ is traditionally used in NFS as a characteristic of the transition state, related to the distance $x^{\ddagger}$ through the replacement $V/V^{\ddagger} \rightarrow \beta F x^{\ddagger}$, where F is the mechanical force. $V^{\ddagger}$ can be expressed in terms of the effective charge of the DNA inside the pore as[19] $V^{\ddagger} = (\beta Q_{\text{eff}})^{-1}$, where $\beta = 1/k_B T$ with k_B being the Boltzmann constant and T the absolute temperature. Even with no voltage applied, the system

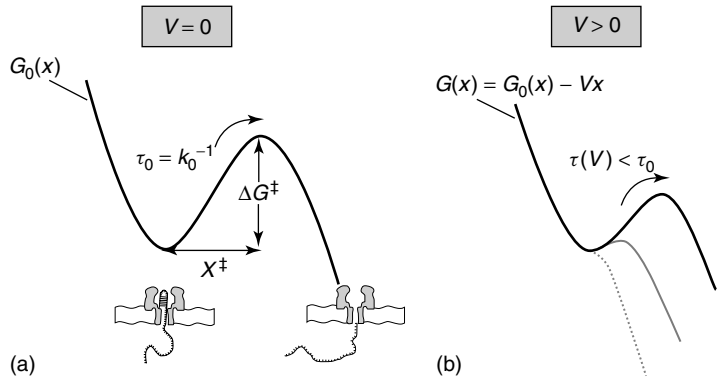

Figure 4 Schematic representation of a single-well free-energy surface. (a) Intrinsic (i.e. zero voltage) free-energy surface $G_0(x)$ with a well (folded state) and a barrier to quasi-irreversible unfolding. In the context of the voltage-driven unzipping of individual DNA hairpin molecules in a nanopore, the well of the free-energy surface corresponds to the single-stranded DNA overhang threaded into the pore constriction with the folded hairpin trapped in the pore vestibule, while escape over the barrier involves the double-stranded part of the DNA being unzipped during its passage through the pore. (b) Free-energy surface $G(x)$ in the presence of an external voltage V. As the voltage increases, both the barrier height and the distance to the transition state decrease (gray line), and both eventually vanish (dotted line), when the well and the barrier merge at a critical voltage.

will eventually escape out of the well over the barrier by thermal activation; the time it takes to do so is related to its characteristic intrinsic lifetime in the well, τ_0.

With applied voltage V, the voltage drop across the membrane-spanning nanopore results in an electric field that generates a force on the charged DNA strand threaded into the nanopore. This force tilts the barrier (Figure 4b), which accelerates the molecular transition because the system diffuses on a combined free-energy surface, $G(x) = G_0(x) - Vx$ that is more favorable to transition than the original free-energy surface $G_0(x)$. The reaction coordinate x represents a measure of the translocation progress along the nanopore axis; in the context of unzipping DNA hairpins, for example, it is defined as the length of the initially double-stranded part of DNA that has advanced past the pore entrance.

Although this formalism assumes a single barrier, it can be applied for each individual transition in the case of multiple populated states, if the states can be resolved experimentally, for example, on the basis of their molecular extensions along the reaction coordinate. The formalism is applicable both to the forward (e.g. unzipping or dissociation) or the backward (e.g. refolding or rebinding) transitions, as long as these transitions are quasi-irreversible.

2.2.1.1 Kinetics Under Constant Voltage The kinetics of rupture is described by the survival probability $S(t)$ or the probability that the system is still intact at time t in a measurement that started at $t = 0$ at constant voltage. When the applied voltage is not too high, in many systems the relaxation to equilibrium in the free-energy well (i.e. in the unruptured state) occurs on a very short timescale compared with the characteristic lifetime in the well, so that the escape over the barrier (i.e. rupture) is considered a rare event. In this case, the survival probability $S(t)$ satisfies a first-order rate equation

$$\dot{S}(t) = -S(t)/\tau(V) \tag{1}$$

where $\dot{S}(t) \equiv \mathrm{d}S/\mathrm{d}t$ and $S(0) = 1$. $\tau(V)$ is the average lifetime of the molecular bond in the presence of a constant voltage V. The solution of Equation (1) is a single-exponentially decaying survival probability, $S(t) = \exp[-t/\tau(V)]$. As shown in Equation (2), the distribution of lifetimes, $p(t) = -\dot{S}(t)$, is then also exponential

$$p(t) = \exp[-t/\tau(V)]/\tau(V) \tag{2}$$

Observation of non-single-exponential rupture kinetics under constant voltage would be an indication of other slow processes present in the system, such as crossing of multiple barriers before the rupture occurs.

Experimentally, the characteristic lifetime $\tau(V)$ can be obtained from the fit of a single-exponential function to the distribution of lifetimes constructed from a sufficient number of individual rupture events based on repeated lifetime measurements (Figure 2b).

2.2.1.2 Kinetics Under Constant Voltage- Ramp If, on the other hand, the applied voltage V (Equation 3) is ramped up linearly with time, and the ramp speed,

$$\dot{V} \equiv \mathrm{d}V/\mathrm{d}t \tag{3}$$

is not too high (within the so-called quasi-adiabatic regime), Equation (1) for the survival probability becomes

$$\dot{S}(t) = -S(t)/\tau[V(t)] \tag{4}$$

where the lifetime $\tau[V(t)]$ depends on the value of the voltage at time t. Note that $\tau(V)$ in Equations (1) and (4) is the same function of voltage. By integration, $S(t) = \exp\left[-\int_0^t \frac{dt'}{\tau[V(t')]}\right]$ is obtained. The distribution of voltages at rupture, which is the typical output in experiments under a constant-voltage ramp, can be obtained from Equation (4) using $p(V) = -\dot{S}/\dot{V}$:

$$p(V) = \frac{\exp\left[-\int_0^V [\dot{V}\tau(V')]^{-1} dV'\right]}{\dot{V}\tau(V)} \tag{5}$$

2.2.1.3 Relating Constant-Voltage Experiments to Voltage-ramp Experiments Equation (5) can be readily inverted[20] to express the lifetime in terms of the rupture-voltage distribution $p(V)$ and loading rate $\dot{V}$:

$$\tau(V) = \frac{\int_V^\infty p(V')dV'}{\dot{V}p(V)} \tag{6}$$

The resulting Equation (6) shows how rupture-voltage distributions $p(V)$ measured at different loading rates $\dot{V}$ (right-hand side of Equation 6) can be directly transformed into the voltage dependence of the lifetime $\tau(V)$ (left-hand side of Equation 6) measurable in constant-voltage experiments. This relation, which is independent of the nature of the underlying free-energy surface, predicts that data obtained at different ramp speeds must collapse onto a single master curve that determines the voltage dependence of the lifetime $\tau(V)$ over a wider range of voltages than may be readily available from constant-voltage experiments. If the data do not collapse, then Equations (1) and (4) do not hold, and the time course of the kinetics at constant voltage is expected to be more complex than a single exponential. The data collapse for DNA hairpin unzipping experiments is illustrated in Section 3.

From Equation (6) an approximate but quite general relationship between the lifetime at a voltage equal to the mean rupture voltage and the variance of the rupture-voltage distribution can be obtained[21]:

$$\tau(\langle V\rangle) \approx \left[\frac{\pi}{2\dot{V}^2}(\langle V^2\rangle - \langle V\rangle^2)\right]^{1/2} \tag{7}$$

Whereas Equation (7) gives an estimate for the $\tau(V)$ over a narrower range of V than does Equation (6), it should prove useful if the data permit estimates of only the mean and variance.

The above mentioned results immediately suggest a remarkably simple approach to the analysis of single-molecule data obtained from NFS experiments under a constant-voltage ramp. If there are sufficient data to construct reasonably ''smooth'' rupture-voltage histograms, one can obtain the lifetimes $\tau(V)$ simply by transforming the histograms according to Equation (6). If limited data allow estimates of only the mean and the variance, Equation (7) can be used to estimate $\tau(V)$ over a narrower range of forces.

2.2.2. *Models for the Kinetics of Rupture Under Applied Voltage*

In the foregoing, no specific functional form for the voltage-dependent lifetime $\tau(V)$ has been assumed. Here the phenomenological model based on Bell's relation for $\tau(V)$ is introduced, and then a simple unified microscopic description of force-induced molecular rupture is considered based on the picture of diffusive barrier crossing in one dimension. Finally, it is show how the developed theoretical framework makes it possible to extract microscopic information from NFS experimental data is shown.

2.2.2.1 Phenomenological Description of the Kinetics of Rupture The phenomenological approach[22] offers a simple framework for the interpretation of NFS results on the basis of the assumption that a constant external voltage decreases the rupture lifetime in a monoexponential manner (Bell's relation)[23]:

$$\tau(V) = \tau_0 \exp(-V/V^\ddagger) \tag{8}$$

where τ_0 and $V^\ddagger$ are the parameters of the system in the absence of an applied voltage.

When the applied voltage is ramped up linearly with time, in Equation 9, the phenomenological expression for the rupture-voltage distribution can be found analytically using Equation (8) in Equation (5):

$$p(V) = (\tau_0\dot{V})^{-1} \exp\left[\frac{V}{V^\ddagger} - \frac{V^\ddagger}{\tau_0\dot{V}}(e^{V/V^\ddagger} - 1)\right] \tag{9}$$

For moderate values of the voltage-ramp speed $\dot{V}$, the mean voltage at rupture, $\langle V\rangle = \int V'p(V')dV'$, and the variance, $\sigma_V^2 = \langle V^2\rangle - \langle V\rangle^2$, are approximately

$$\langle V\rangle \approx V^\ddagger \ln(\dot{V}e^{-\gamma}\tau_0/V^\ddagger),\ \sigma_V^2 \approx \pi^2 V^{\ddagger 2}/6 \tag{10}$$

where $\gamma \approx 0.5772$ is the Euler–Mascheroni constant. The mode of the rupture-voltage distribution, corresponding to the most-probable voltage with $dp(V)/dV = 0$, is given by the first expression in Equation (10) with γ formally set to zero.

As can be seen in Equation (10), within the framework of the phenomenological approach, the mean (or alternatively, the most probable) rupture voltage is predicted to be a linear function of the logarithm of the ramp speed $\dot{V}$, whereas the variance of the rupture-voltage distribution is essentially independent of the ramp speed.

With the increasing dynamic range of experiments (broader range of $\dot{V}$ values), deviations from this predicted behavior have been observed: The most-probable rupture voltage is found to be not perfectly linear in $\ln \dot{V}$, and the variance of rupture voltages shows increase with the ramp speed $\dot{V}$ rather than remaining constant. Such deviations have often been interpreted as a change in mechanism (e.g. switching from one dominant barrier to another, rebinding). However, as is shown in the following subsection, simple microscopic models with a *single* free-energy minimum (like that depicted in Figure 4) can explain nonlinearity of $\langle V \rangle$ versus $\ln \dot{V}$ plots without introducing additional assumptions about a change in mechanism.[24,25] Simulations of simple models also showed that even in cases where the phenomenological formalism fits the data well, the parameters extracted from the fit can be off substantially from the actual values (e.g. by more than an order of magnitude for the lifetime).[20,24]

The reason for these limitations of the phenomenological approach is the underlying assumption in Bell's formula (Equation 8) that the characteristic of the transition state $V^{\ddagger}$ (which can be visualized as the well-to-barrier distance $x^{\ddagger}$, as shown in Figure 4) is independent of voltage. This assumption cannot be true for all voltages: As can be readily seen by examining the behavior of any smooth one-dimensional potential (Figure 4), the barrier and the well must move closer (solid gray line in Figure 4b) as the voltage increases, because they eventually merge (dotted line in Figure 4b) at a critical voltage when the barrier to rupture vanishes. As a result, $\ln \tau(V)$ must be a nonlinear function of V, in contrast to the assumption made in Equation (8).

2.2.2.2 From Microscopic Models to Unified Theory of the Kinetics of Rupture Simple, analytically tractable microscopic models of molecular rupture in the presence of a bias field (e.g. a voltage gradient) can be constructed on the basis of Kramers theory for the lifetime $\tau(V)$ in a free-energy minimum in one dimension. These microscopic models remove the restrictive assumption of a voltage-independent transition state location postulated by the phenomenological Equation (8), yet they lead to analytical expressions for experimental observables, such as the lifetime at constant voltage and the rupture-voltage distribution in the presence of a time-varying external voltage.

Consider diffusive dynamics on a one-dimensional free-energy surface $G(x) = G_0(x) - Vx$ with an effective diffusion coefficient D, where $G_0(x)$ is the profile in the absence of voltage. Instead of using Equation (8) for the bond lifetime, as is done in the phenomenological approach, one can specify the free-energy surface $G_0(x)$ and use the Kramers theory,[26,27] which, for sufficiently high barriers separating the unruptured states from the ruptured states, predicts

$$\tau(V) = D^{-1} \left(\int_{\ddagger} \mathrm{e}^{\beta \mathrm{G(x)}} \mathrm{d}x \right) \left(\int_{\mathrm{well}} \mathrm{e}^{-\beta \mathrm{G(x)}} \mathrm{d}x \right) \qquad (11)$$

where the first integral is taken over the barrier region, and the second integral is taken over the free-energy minimum of $G(x)$.

There are at least two single-well models of the free-energy surface $G_0(x)$ for which the closed-form analytical expressions for NFS experimental observables can be derived, both for constant voltage and for constant-ramp regimes: a linear–cubic surface $[G_0(x) = (3/2)\Delta G^{\ddagger} x/x^{\ddagger} - 2\Delta G^{\ddagger}(x/x^{\ddagger})^3]$ and a harmonic–cusp surface $[G_0(x) = \Delta G^{\ddagger}(x/x^{\ddagger})^2$ for $(x < x^{\ddagger})$ and $-\infty$ for $(x \geq x^{\ddagger})]$. The general nature of the linear–cubic model becomes evident as soon as one realizes that for high enough forces the cubic polynomial forms a natural Taylor-series approximation to any smooth combined free-energy surface.[20] In the same time, assumption of a cusplike barrier in the harmonic–cusp model is justified by the fact that, because of the snapping motion at rupture, experiments contain limited information about the shape of the free-energy surface near the transition state. When calculated using Kramers theory (Equation 11), the lifetime $\tau(V)$ for these two models (linear–cubic and harmonic–cusp) can be expressed in terms of the three *zero-voltage* parameters: intrinsic lifetime τ_0, distance $x^{\ddagger}$ to the transition state from the well center (or, alternatively, the characteristic voltage $V^{\ddagger}$ traditionally used in NFS to describe the transition state), and the activation-free energy $\Delta G^{\ddagger}$. Furthermore, the final results of all three approaches (phenomenological, linear–cubic and harmonic–cusp) can be unified.[20] Specifically, the lifetime at constant voltage can in all three cases be written as

$$\tau(V) = \tau_0 \left(1 - \frac{\mu V}{\beta \Delta G^{\ddagger} V^{\ddagger}} \right)^{1-1/\mu} \times \exp \left\{ -\beta \Delta G^{\ddagger} \left[1 - \left(1 - \frac{\mu V}{\beta \Delta G^{\ddagger} V^{\ddagger}} \right)^{1/\mu} \right] \right\} \qquad (12)$$

The scaling parameter μ specifies the model: $\mu = 2/3$ and $\mu = 1/2$ correspond to the linear–cubic potential and harmonic–cusp potential, respectively. For $\mu = 1$, or

for $\Delta G^{\ddagger} \to \infty$ independent of μ, the phenomenological expression (Equation 8 is recovered from Equation 12). For $\mu \neq 1$, Equation (12) becomes invalid when V approaches the critical voltage $V_c = \beta \Delta G^{\ddagger} V^{\ddagger}/\mu$ at which the barrier to rupture vanishes. This problem is caused by the use of the Kramers high-barrier approximation, and can be circumvented by using the full mean-first-passage times formula to determine the voltage-dependent lifetime.[28]

When the voltage is ramped up linearly with time, the distribution of voltages at rupture is obtained by using Equation (12) in Equation (5):

$$p(V) = (\tau(V)\dot{V})^{-1} \times \exp\left\{\frac{V^{\ddagger}}{\tau_0 \dot{V}}\left[1 - \frac{\tau_0}{\tau(V)}\left(1 - \frac{\mu V}{\beta \Delta G^{\ddagger} V^{\ddagger}}\right)^{1-1/\mu}\right]\right\} \tag{13}$$

where $\tau(V)$ is the voltage-dependent lifetime of Equation (12). The average of the rupture voltage is approximately

$$\langle V \rangle \approx \frac{\beta \Delta G^{\ddagger} V^{\ddagger}}{\mu}\left\{1 - \left[\frac{1}{\beta \Delta G^{\ddagger}} \ln \frac{V^{\ddagger} e^{\beta \Delta G^{\ddagger} + \gamma}}{\tau_0 \dot{V}}\right]^{\mu}\right\} \tag{14}$$

where $\gamma \approx 0.5772$ is the Euler–Mascheroni constant. Once again, when γ is formally set to zero, Equation (14) closely approximates the most-probable rupture voltage (i.e. mode of the distribution). The variance of the rupture-voltage distribution is

$$\sigma_V^2 \approx \frac{\pi^2 V^{\ddagger 2}}{6}\left[\frac{1}{\beta \Delta G^{\ddagger}} \ln \frac{V^{\ddagger} e^{\beta \Delta G^{\ddagger} + \tilde{\gamma}}}{\tau_0 \dot{V}}\right]^{2\mu - 2} \tag{15}$$

Here $\tilde{\gamma} = \gamma^2 - 3/\pi^2 \psi''(1) \approx 1.064$.

Equations (12–15) provide analytical expressions for the experimental observables in NFS in terms of the intrinsic (zero force) parameters of the system, τ_0, $V^{\ddagger}$, and $\Delta G^{\ddagger}$. The above-mentioned results, based on a class of microscopic models of force-induced crossing of a single barrier, show that logarithm of the lifetime, $\ln \tau(V)$, is a nonlinear function of the applied voltage (Equation 12 with $\mu \neq 1$). This nonlinear dependence is a simple consequence of the fact that the distance to the transition state decreases as the force increases, eventually vanishing when the barrier disappears (Figure 4b). Hence, in a constant voltage-ramp experiment, the average rupture voltage $< V >$ will depend nonlinearly on the logarithm of the ramp speed, $\ln \dot{V}$ (Equation 14 with $\mu \neq 1$). Because this property of the transition state is ignored in the phenomenological model (corresponding to $\mu = 1$ in Equations 12–15), the latter can capture the quantitative behavior of the experimental observables only in the limited regime of low voltages, and its imprudent use in fitting experimental data can lead to significant errors in estimated parameters of the system.

2.2.3 *Analysis of NFS Experiments*

2.2.3.1 *Analysis of Constant-Voltage Experiments*

Voltage dependence of the lifetime obtained in constant-voltage measurements can be interpreted in microscopic terms simply by least-squares fitting the data to Equation (12) at several fixed values of μ. If the resulting parameters τ_0, $V^{\ddagger}$, and $\Delta G^{\ddagger}$ are relatively insensitive to μ in the range of $1/2 \leq \mu \leq 2/3$ and thus to the precise shape of the underlying free-energy surface, these parameters may be considered meaningful. Alternatively, as discussed in Dudko et al.,[21] a generalization of the Equation (8) that is formally exact within the framework of Kramers theory can be used to extract information about the transition state as a function of voltage from the lifetimes, *independent* of the shape of the free-energy surface.

2.2.3.2 Analysis of Voltage-ramp Experiments There are two complementary approaches to extracting microscopic information from rupture-voltage distributions obtained in a constant voltage-ramp experiment. In the first approach, a maximum-likelihood (ML) formalism is used to fit to Equation (13) all rupture-voltage histograms collected at one or (preferably) several voltage-ramp speeds $\dot{V}$. In the second approach, rupture-voltage histograms are transformed according to Equation (6) into the voltage dependence of the lifetime, from which analysis may proceed as described in the subsection titled ''analysis of constant-voltage experiments'' earlier. Implementation of these two approaches is discussed below.

2.2.3.3 Maximum Likelihood Analysis of Constant Voltage-ramp Experiments Consider a series of constant voltage-ramp speed experiments at several ramp speeds $\dot{V}_j (j = 1, \ldots, N)$. Molecular rupture will be observed at different voltages V_{ij} $(i = 1, \ldots, M_j)$. The likelihood function L needs to be maximized with respect to a set of model parameters $\{\alpha\}$. L can be expressed in terms of the rupture-voltage distribution $p(V|\dot{V})$ at ramp speed $\dot{V}$ as

$$L = \prod_{j=1}^{N} \prod_{i=1}^{M_j} p(V_{ij}|\{\alpha\}; \dot{V}_j) \tag{16}$$

To implement this approach, it is convenient to have an analytical expression for $p(V|\dot{V})$. The unified formalism described earlier provides such an expression

in Equation (13) in terms of the model parameters such as intrinsic lifetime τ_0, characteristics of the transition state $V^{\ddagger}$, and the activation-free energy $\Delta G^{\ddagger}$. Given experimental measurements, optimal values of τ_0, $V^{\ddagger}$, and $\Delta G^{\ddagger}$ can be found by maximizing L or, equivalently, $\ln[L]$ for different fixed values of μ. As in the case of the constant-voltage data analysis, if the resulting parameters $\{\tau_0, V^{\ddagger}, \Delta G^{\ddagger}\}$ are relatively insensitive to the value of μ in the range $1/2 \leq \mu \leq 2/3$, they can be considered meaningful.

2.2.3.4 Transformation of Rupture-voltage Histograms into Voltage Dependence of Lifetime The histogram transformation approach is based on the mapping equation, Equation (6), which transforms rupture-voltage histograms measured at different voltage-ramp speeds directly into voltage dependence of the rupture lifetime. This approach is simpler to implement than a global ML fit of all available histograms, but it is less rigorous, and requires binning data.

The transformation of histograms using Equation (6) is implemented as follows. Consider a rupture-voltage histogram at the voltage-ramp speed $\dot{V}$. The histogram contains N bins of width ΔV, starts at V_0 and ends at $V_N = V_0 + N\Delta V$, and has N_{tot} total number of counts. Let the number of counts in the ith bin be C_i, resulting in a height $p_i = C_i/(N_{\text{tot}}\Delta V)$ in the normalized voltage distribution. Then, the lifetime at the voltage $V_0 + (k - 1/2)\Delta V$ is

$$\tau(V_0 + (k-1/2)\Delta V) = \frac{\left(p_k/2 + \sum_{i=k+1}^{N} p_i\right)\Delta V}{\dot{V}\, p_k} \qquad (17)$$

where $k = 1, 2, \ldots$ Equation (17) is simply a discrete version of Equation (6).

If the histograms do collapse onto a single master curve, one immediately obtains the voltage dependence of bond lifetime, $\tau(V)$, or equivalently, the rate of rupture under voltage, $k(V) = 1/\tau(V)$. The voltage dependence of the lifetime can now be interpreted in microscopic terms in exactly the same way as the lifetimes that were measured directly in constant-voltage experiments, by simply performing a least-squares fit to Equation (12), or by using a model-independent approach as discussed in Dudko et al.[21]

If the histograms transformed by Equation (17) do not collapse onto a single master curve, then the mechanism of rupture cannot be described as an irreversible, quasi-adiabatic escape over a single barrier. Such behavior may also be evident in nonexponential distributions of the lifetimes in constant-voltage experiments.

3 ILLUSTRATIVE APPLICATION – BOND BREAKAGE INVESTIGATED BY NANOPORE FORCE SPECTROSCOPY: CASE OF INDIVIDUAL DNA UNZIPPING

The unzipping of double-stranded nucleic acids is a fundamental process from the point of view of molecular genetics. It is involved in DNA replication, RNA transcription, translation initiation, and RNA interference, as well as many other cellular processes. The forces and timescales associated with the breakage of the bonds stabilizing the secondary and tertiary structures of nucleic acids can now be studied at the single-molecule level, revealing information masked heretofore by ensemble averaging, including short-lived intermediate states and multistep kinetic processes. In particular, nanopores can be used to directly apply and measure unzipping forces on individual DNA and RNA molecules, eliminating the need for molecular linkers, for surface immobilization of the molecules, and for global application of force.

The protein pore alpha-hemolysin (α-HL) is nearly ideal for nucleic acid unzipping studies. Its heptameric structure,[29] composed of cap and stem portions, has been shown to be highly stable even under high temperatures, voltage gradients,[30] and a wide range of ionic strengths (i.e. 0.25 M−2 M KCl).[31] The cap portion of α-HL, which is usually assembled on the "*cis*" side of the membrane, contains a wide vestibule like mouth, which can accommodate double-stranded nucleic acids. The stem portion, which spans the phospholipid membrane, is nearly a cylindrical water-filled channel with an inner diameter ranging from 1.4 to 1.8 nm.[29] It therefore geometrically permits the passage of ssDNA or ssRNA molecules, but blocks the translocation of double-stranded nucleic acids.

Sauer-Budge et al. demonstrated that a DNA duplex molecule (composed of a 100-mer oligo hybridized to a matching 50-mer oligo, such that a 50-mer 3′ single-stranded overhang is formed), must be unzipped when the 3′ overhang is threaded through the pore.[32] A quantitative polymerase chain reaction (PCR) analysis showed that while both the 50-mer and 100-mer oligos were present in the *cis* chamber, only the 100-mer oligo was found in the *trans* chamber, after the detection of hundreds of nanopore blockade events. The most plausible explanation for this observation was that unzipping had occurred at the pore, leaving all 50-mer oligos in the *cis* chamber while the 100-mer oligos passed through the pore to the *trans* side.[32] Furthermore, the distribution of nanopore blockade durations (or dwell times) displayed a characteristic mean time of ∼435 ms, orders of magnitude longer than the timescale associated with the translocation of ssDNAs of comparable length.

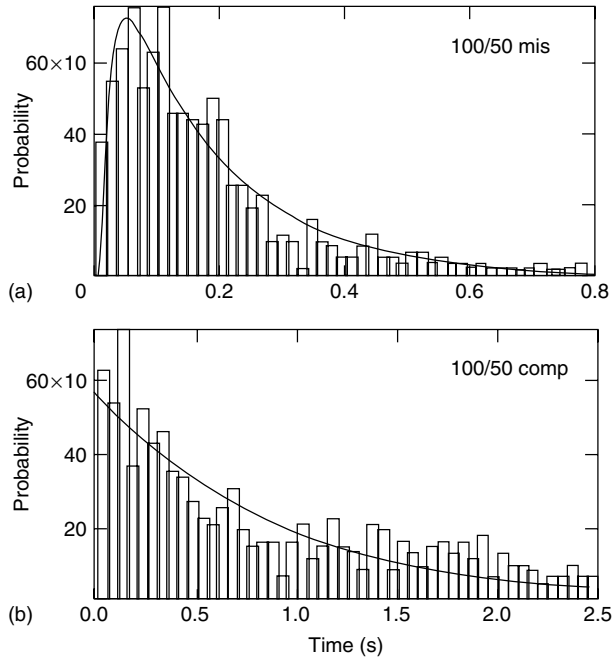

Figure 5 Dwell time distributions of unzipping events of a 50/100 DNA hybrid, with 6-base mismatch (top) and perfect match (bottom). The mismatch events yield a characteristic timescale shorter by roughly a factor of 2 (185 ms vs. 435 ms). (Reproduced with permission from Ref. 32).

Introducing a 6-base mismatch in the duplex region of the hybridized sample, resulted in a shortening of the characteristic timescale by more than a factor of two[32] (Figure 5).

While these experiments provided the first evidence that the α-HL pore can be used to unzip DNA duplexes, they were limited to a narrow range of voltages (120–180 mV), making it difficult to precisely determine the kinetic properties of the process. One of the difficulties with static-voltage measurements is that the event rate (the rate at which new molecules enter the pore) depends exponentially on the applied voltage,[33,34] making it impractical to perform measurements at low voltages (i.e. below ~100 mV). Although using higher static voltages would improve the pore's capture rate, they would also cause faster translocations and faster unzipping, which might not be detectable within experimental bandwidth. This problem is solved by dynamic voltage control (DVC), which allows one to apply different voltage levels for the threading and unzipping processes.[18] DVC thus enables the study of the unzipping kinetics over a much wider range of voltages using time-varying voltage profiles without compromising the statistical accuracy of the data set.

Mathé et al. employed DVC to study the unzipping properties of DNA hairpin molecules.[19,35] They systematically probed the distributions of unzipping times of three DNA hairpin molecules composed of duplex regions (10 bp, 9 bp, or 7 bp) and a 3′ poly(dA)$_{50}$ ssDNA overhang, over a wide range of both voltage (30–150 mV) and temperatures. Figure 2 (see previous) displayed an example of a typical unzipping event using DVC and a voltage step, and the corresponding distribution of ~1500 unzipping events used to determine the characteristic unzipping time, τ_U. These and other measurements revealed that a single-base mismatch (in the 10 bp hairpin) strongly shifts the unzipping timescale (τ_U) toward shorter times and can therefore be easily detected, as shown in Figure 6. They demonstrated that single-nucleotide mutations can be detected in both DNA hairpins and in DNA hybrids.

The cumulative unzipping time distributions could be fit, to good approximation, using first-order rate kinetics (monoexponential functions), shown as dashed line in Figure 6. The dependence of the characteristic unzipping timescale, τ_U, on voltage V is shown as a semilog plot in Figure 7. To first approximation, all data points can be fitted using monoexponential functions *with the same slope*. If the unzipping process using the phenomenological expression is described in Equation (8), this implies that the amount by which the energy barrier is reduced because of the electrical force is uniform (among different hairpins) and can be used to define a universal effective charge Q_{eff}. For the data shown in Figure 7, this effective charge is roughly ~0.1 e per nucleotide in close agreement with initial studies by Sauer-Budge et al.[32]

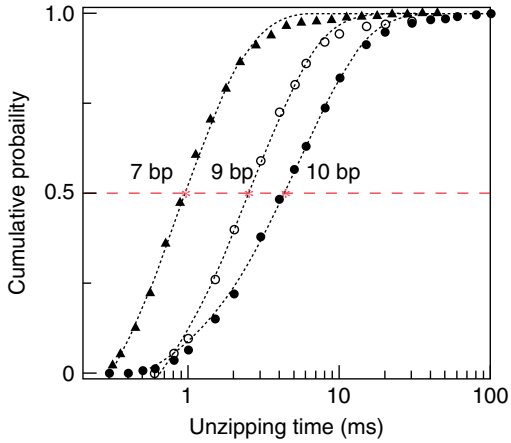

Figure 6 Detecting single-base mismatches in unlabeled DNA hairpins. The normalized cumulative distributions of the unzipping time measured using DVC at 120 mV and 15 °C, for 10 bp, 9 bp (10 bp with a mismatch), and 7 bp DNA hairpins (solid circles, empty circles, and triangles, respectively). Monoexponential probability distribution fits (dashed lines) yield characteristic unzipping timescales (~5 ms, 3 ms, and 1 ms for the 10 bp, 9 bp, and 7 bp, respectively) used to discriminate between the hairpins.

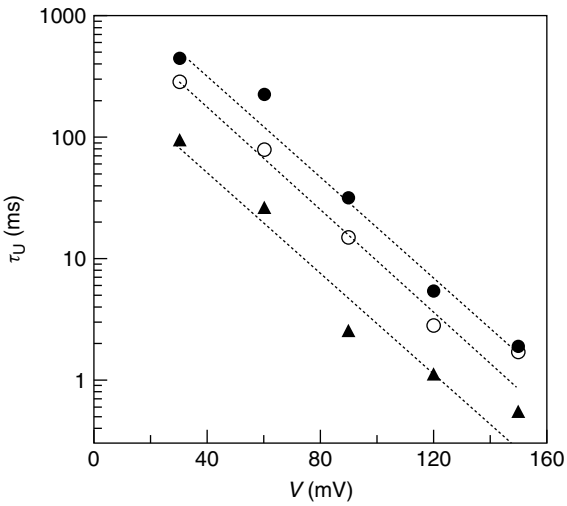

Figure 7 Dependence of the characteristic unzipping timescale on the voltage measured using DVC, for 10 bp, 9 bp (10 bp with a mismatch), and 7 bp DNA hairpins (solid circles, empty circles, and triangles, respectively). As a first approximation, all molecules follow a monoexponential dependence on V with the same slope. (Reproduced with permission from Ref. 19).

DNA hairpin unzipping measurements were also performed using voltage-ramp measurements, as explained in Figure 3. ML analysis and Equation (13) may be directly applied to such NFS voltage-ramp data, as discussed later. There are a number of practical advantages to using a voltage ramp over constant-voltage measurements. Most importantly, it turns out that constant-voltage unzipping is a much more time-consuming measurement as compared with voltage-ramp unzipping. This is a direct consequence of the fact that the unzipping distributions obtained in the voltage-ramp method depend, to a first approximation, logarithmically on the ramp, whereas the unzipping time distributions obtained in the constant-voltage method depend roughly exponentially on the applied voltage. The next section demonstrates how to transform, using Equation (6), the voltage-ramp data directly into voltage dependence of the unzipping times measurable at constant voltage.

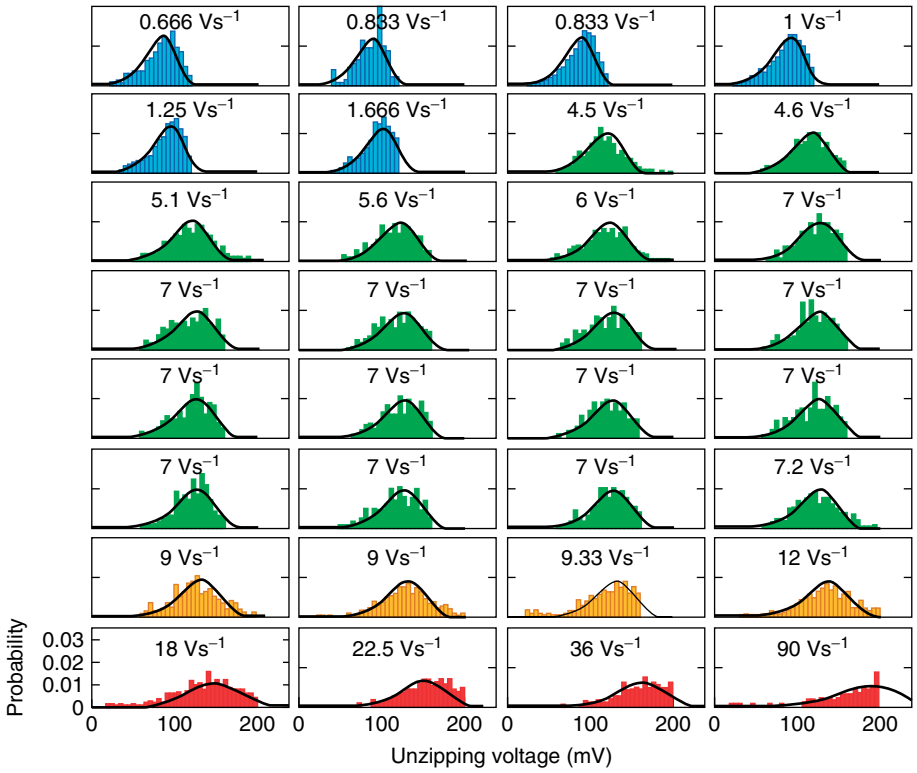

Figure 8 Distribution of the unzipping voltage from experiment (histograms) and theory (lines). Theoretical distributions were obtained by ML global fit of histograms at ramp speed of 12 V/s or less to Equation (13) with $\mu = 2/3$ (linear–cubic model); the result for $\mu = 1/2$ (linear–cubic model, not shown) is very similar. The likelihood function, Equation (16), was maximized numerically with respect to the model parameters. Experimental data collected at ramp speeds above 12 V/s (in this regime, the DNA hairpin was still intact when the maximum voltage 0.2 V had been reached) were not used in the fit and instead were set aside for subsequent validation. The microscopic theories reproduce the measured distributions of unzipping voltages very well both in the regime used for the fit and outside that regime. The phenomenological model (fit not shown) with the estimates obtained from the global ML fit was found to be accurate at low ramp speeds, whereas at higher speeds the deviations were substantial. Colors reflect different ranges of the ramp speed and correspond to those in Figures 9 and 10.

3.1 Maximum-Likelihood Analysis of Voltage-Ramp Data

Over 32 independent DNA hairpin unzipping data sets, obtained for different ramp values as explained in Figure 3, were used to form voltage histograms and were globally fitted using Equation (13) by maximizing the likelihood function, Equation (16). Figure 8 displays the result of the fits. Colors represent four ranges of the voltage-ramp level (see caption). As summarized in Table 1, the two microscopic theories ($\mu = 2/3$ and $\mu = 1/2$ in Equation 13) produce consistent estimates for the model parameters. ML fitting parameters of the phenomenological theory ($\mu = 1$ in Equation (13)) are also included for comparison.

Figure 9 shows the most-probable unzipping voltage V_m as a function of the voltage-ramp speed. The markers represent the experimental data, and the solid line is the theoretical prediction using microscopic theory (Equation 14 with γ set to 0 and $\mu = 2/3$) with ML parameters (Table 1). Additionally, we show as a dashed line the phenomenological prediction obtained from the fit of V_m to Equation (14) (with γ set to 0 and $\mu = 1$) at the intermediate and high voltages. To explain the observed curvature in the data for the most-probable unzipping voltage versus log $\dot{V}$, the phenomenological model (predicting the linear behavior of the mode vs. log-ramp speed) requires the assumptions of additional molecular processes, such as hairpin rezipping or switching between multiple states, which cannot be captured by the single-well energy landscape drawn in Figure 4. In contrast, as can be seen in Figure 9, the microscopic theory captures the nonlinearity of the most-probable unzipping voltage in log $\dot{V}$ even though this theory makes no assumptions beyond a single-well energy landscape. Additionally, it can be verified[28] that the variance σ_V^2 of the unzipping voltage distributions exhibits a noticeable increase in the ramp speed, in agreement with the microscopic theories (Equation 15 with $\mu = 1/2$ and $\mu = 2/3$).

3.1.1 *Histogram Transformation Method*

Quantitatively relating the constant-voltage data to the voltage-ramp data using Equation (6) and its discrete analogue, Equation (17), provides a simple way to obtain the voltage-dependent lifetime $\tau(V)$ directly from the voltage-ramp data. Figure 10 is an illustration of the utility of Equation (6) for this system. Not only do the $\tau(V)$ obtained from histograms at different ramp speeds collapse onto the same curve (colored symbols), but there is also excellent agreement with DNA unzipping lifetimes obtained by an *independent set of measurements* of $\tau(V)$ using constant voltages (open circles). The $\tau(V)$ obtained from the mean and variance using Equation (7) (filled circles) are also found to agree with the constant-voltage experiments.

Now that the voltage dependence of the lifetime has been obtained from rupture-voltage histograms, the procedure of interpreting this dependence in microscopic terms can be implemented. It is clear from Figure 10 that deviations from the monoexponential dependence of the lifetime on the voltage (Equation 8) are present when the voltage exceeds ~125 mV. The microscopic models allow us to perform a least-squares fit of the data to Equation (12) over the entire range of accessible voltage, producing the following kinetic parameters: $\tau_0 = 14.3\,\text{s}$, $V^\ddagger = 11.1\,\text{mV}$, and $\Delta G^\ddagger = 11.9\,k_B\text{T}$ for $\mu = 1/2$, and $\tau_0 = 9.6\,\text{s}$, $V^\ddagger = 12.8\,\text{mV}$, and $\Delta G^\ddagger = 10.4\,k_B T$ for

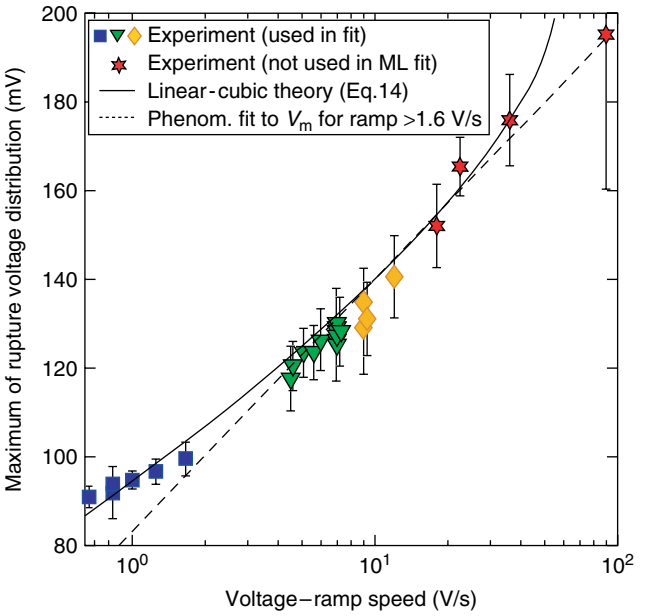

Figure 9 Dependence of the maximum V_m of the unzipping voltage distribution on the voltage-ramp speed from experiment (markers) and theory (lines, Equation 14 with γ set to 0). Model parameters for the linear–cubic theory (solid line, Equation 14 with $\mu = 2/3$) were obtained from global ML fit, see Figure 8 and Table 1; result for the harmonic–cusp theory (Equation 14 with $\mu = 1/2$, not shown) is very similar. Dashed line is the least-squares fit of the maximum of unzipping voltage distributions to the phenomenological model (Equation 14 with $\mu = 1$) for ramp speeds >1.6 V/s. Color coding as in Figure 8.

Table 1 Maximum-likelihood estimates for the kinetic parameters for nanopore unzipping of DNA. Estimates were obtained from data in Figure 8 at ramp speeds 12 V/s or less by maximizing the likelihood function in Equation (16) with the expression in Equation (13) for the unzipping voltage distributions

μ	$V^\ddagger$ (mV)	$\Delta G^\ddagger$ (k_BT)	τ_0 (s)
1	21.7	–	1.6
2/3	12.7	10.5	8.3
1/2	9.9	11.9	20

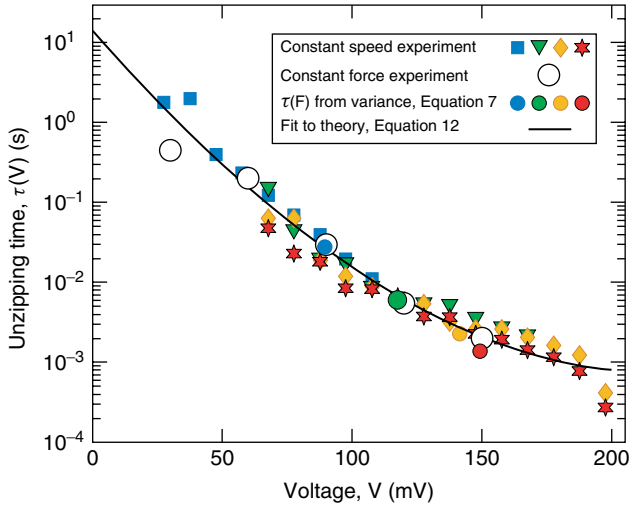

Figure 10 Lifetime $\tau(V)$ of the DNA hairpin as a function of the applied voltage V. The lifetime is obtained by transforming the four representative rupture-voltage histograms for ramp speeds from 0.83 V/s to 18 V/s (filled symbols, colors as in Figures 8 and 9) according to Equation (6). Least-squares fit of the collapsed histograms to Equation (12) with $\mu = 1/2$ is shown as line; the fit with $\mu = 2/3$ (not shown) is comparable. Note the agreement with the lifetimes measured directly at constant voltage (open circles).

$\mu = 2/3$, in a good agreement with the values of the ML global analysis in Table 1. Collapsed data collected at different ramp speeds probe different ranges of the DNA unzipping lifetime $\tau(V)$. Taken together, they span four orders of magnitude of the bond-rupture lifetime. Furthermore, Figure 10 shows that, although constant-voltage data (open circles) were not used in the fit, the data are actually accurately predicted by Equation (12).

It can be verified[21] that the microscopic theory in Equation (13) is able to accurately *predict* the original rupture-voltage distributions when the parameters of the least-squares fit of the collapsed distributions to Equation (12) are used. Thus, in this case, the histogram transformation procedure gives essentially the same information as the more-sophisticated ML method, but is simpler to implement.

4 CONCLUSIONS AND SUMMARY

Force spectroscopy of individual biomolecules and biomolecular complexes can provide direct insight into the strength of molecular bonds and their stability under stress. Single-molecule techniques such as AFM and optical or magnetic tweezers, are currently the most direct methods of applying and measuring forces on biomolecules, and thus have been broadly employed for studying a wide range of biological systems. These methods, however, require that biomolecules are chemically grafted onto solid surfaces or beads, which limit their throughput, and apply a global mechanical force to the molecule, which complicates investigation of local interactions. NFS utilizes the native electric charge of virtually any biomolecule to exert forces when a biomolecule is threaded through a single-nanoscale constriction. Nanopores do not require the formation of a physical attachment between the biomolecules and the pore, and force is not applied to the entire molecule at once. Rather, the pore constriction itself exerts a shear force on those parts of the biomolecular complex that do not fit inside the pore. NFS utilizes these advantages to locally rupture bonds and directly measure $\tau(V)$ and $p(V)$, two important indicators of bond stability.

The process of bond rupture is most commonly described by an energy-barrier crossing, where the bound state refers to the unperturbed system and the unbound state describes the ruptured bond. Appropriate ruptures of bonds represent fundamental steps in most biomolecular processes. In many cases, the bound and unbound states are separated by a large energy barrier (many k_BTs), and the system remains stable over long periods of time. The energy-barrier height and thus bond stability is reduced by an external application of force, effectively catalyzing the molecular transition. Force spectroscopy probes a system's response over a broad spectrum of forces by measuring either the distribution of bond-rupture transition times at each given force or the rupture-force distribution at a given force ramp speed. Either measurement allows mapping of the system's energy landscape, and extrapolation of the equilibrium transition rate using the nonequilibrium transition rate.

To interpret the experimental outputs in terms of the underlying molecular properties, a unified theory has been developed for a class of single-barrier free-energy landscape models. This theory yields closed-form analytical solutions for the experimental observables, which readily enable fitting the voltage-dependent bond lifetimes measured for constant force (Equation (12)) and employing the powerful ML analysis of the rupture-voltage distributions measured for a constant force ramp (Equation (13)). As a result, intrinsic physical parameters characterizing the system can be extracted, namely, the activation energy-barrier height, its position with respect to the bound state, and the lifetime characterizing the system. Studies show that the rupture-voltage histograms obtained at different voltage-ramp speeds can be transformed to determine the voltage-dependence of the bond lifetimes measurable at constant voltage (Equation 6). This transformation is independent of the functional form of the free-energy landscape and is valid if rupture-voltage kinetics at constant force is well represented by a single exponential. Although this

formalism was developed to describe irreversible rupture, it is applicable to both forward and reverse transitions as long as they can be resolved experimentally.

In this article, we have illustrated the principles of NFS by focusing on DNA hairpin unzipping kinetics. It is shown that the constant pulling voltage and steady voltage-ramps experiments can be mapped on the same rupture time versus voltage curve (Figure 10) that can be described by a unified theory (Equation (12)), providing insight on the system's underlying energy landscape. The NFS method is quite general and has already been applied for other biomolecular systems. For example, Hornblower et al. have recently used NFS to study the interactions of Exonuclease I with ssDNA molecules.[36] NFS data can be extrapolated to zero voltage (or zero force) and be used to measure the dissociation and association constants of the system. Although most of the work presented here focused on the use of protein pores, specifically α-HL, the fragility of the bilayer membrane has limited these measurements to relatively small forces (few tens of pN). A wider range of biomolecular complexes, such as long DNA or RNA molecules or proteins can be studied using NFS if this limitation is removed. The recent progress in fabrication and characterization of synthetic nanopores, specifically nanopores made in thin inorganic membranes,[37,38] have generated vast possibilities for NFS. The solid-state nanopores offer superior mechanical, electrical, and chemical robustness over lipid bilayers used with biological pores. Thus, larger voltage and force ranges and a variety of chemical conditions, including extreme pH or denaturants could be used.[11,39] Additionally, solid-state nanopore can now be tailored to any desired dimension, down to $\sim$1 nm.[40] Thus, a much broader range of bimolecular complexes can be used, under broader experimental conditions.[41–46] These developments will undoubtedly be employed for high-throughput NFS analyses of a broad range of biological systems.

ACKNOWLEDGMENTS

The authors acknowledge fruitful collaboration and discussions with Jerome Mathé, Yitzhak Rabin, Mark Akeson, Gerhard Hummer, Attila Szabo, Breton Hornblower, and Anatoly Kolomeisky. They thank Attila Szabo, Allison Squires, and Jianxun Lin for their constructive and insightful comments on this manuscript. O.K.D. was supported by the National Science Foundation CAREER Award (MCB-0845099) and by the Center for Theoretical Biological Physics, National Science Foundation Grant (PHY-0822283). A.M. acknowledges grants support from the National Science Foundation (PHY-0646637), the National Institute of Health (HG-004128 and GM-075893) and Human Frontier Science Program (RGP0036). O. K. D. is a Hellman Faculty Fellow.

ABBREVIATIONS AND ACRONYMS

AFM	Atomic Force Microscope
α-HL	Alpha-hemolysin
DVC	Dynamic Voltage Control
ML	Maximum-Likelihood
NFS	*Nanopore Force Spectroscopy*
PCR	Polymerase Chain Reaction
ss	single-strand

REFERENCES

1. E.L. Florin, V.T. Moy, H.E. Gaub, 'Adhesion Forces Between Individual Ligand-receptor Pairs', *Science*, **264**, 415–417 (1994).
2. M. Gautel, F. Oesterhelt, J.M. Fernandez, H.E. Gaub, 'Reversible Unfolding of Individual Titin Immunoglobulin Domains by AFM', *Science*, **276**, 1109–1112 (1997).
3. M.S.Z. Kellermayer, S.B. Smith, H.L. Granzier, C. Bustamante, 'Folding-unfolding Transitions in Single Titin Molecules Characterized with Laser Tweezers', *Science*, **276**, 1112–1116 (1997).
4. R. Merkel, P. Nassoy, A. Leung, K. Ritchie, E. Evans, 'Energy Landscapes of Receptor-ligand Bonds Explored with Dynamic Force Spectroscopy', *Nature*, **397**, 50–53 (1999).
5. P.E. Marszalek, H. Lu, H. Li, M. Carrion-Vazquez, A.F. Oberhauser, K. Schulten, J.M. Fernandez, 'Mechanical Unfolding Intermediates in Titin Modules', *Nature*, **402**, 100–103 (1999).
6. J. Liphardt, B. Onoa, S.B. Smith, I.J. Tinoco, C. Bustamante, 'Reversible Unfolding of Single RNA Molecules by Mechanical Force', *Science*, **292**, 733–737 (2001).
7. M. Schlierf, H.B. Li, J.M. Fernandez, 'The Unfolding Kinetics of Ubiquitin Captured with Single-molecule Force-clamp Techniques', *Proc. Natl. Acad. Sci. U.S.A*, **101**, 7299–7304 (2004).
8. C. Cecconi, E.A. Shank, C. Bustamante, S. Marqusee, 'Direct Observation of the Three-state Folding of a Single Protein Molecule', *Science*, **309**, 2057–2060 (2005).
9. M. Schlierf, M. Rief, 'Single-molecule Unfolding Force Distributions Reveal a Funnel-shaped Energy Landscape', *Biophys. J.*, **90**, L33–L35 (2006).
10. W.J. Greenleaf, K.L. Frieda, D. Foster, M.T. Woodside, S.M. Block, 'Direct Observation of Hierarchical Folding in Single Riboswitch Aptamers', *Science*, **319**, 630–633 (2008).

11. M. Wanunu, A. Meller, Single-molecule analysis of nucleic acids and DNA-protein interactions using nanopores. *Single-Molecule Techniques: A Laboratory Manual*, eds. P. Selvin, T.J. Ha, Cold Spring Harbor Laboratory Press, Cold Spring Harbor, 395–420 2008.
12. J. Kasianowicz, E. Brandin, D. Branton, D. Deamer, 'Characterization of Individual Polynucleotide Molecules using a Membrane Channel', *Proc. Natl. Acad. Sci. U.S.A.*, **93**, 13770–13773 (1996).
13. M. Akeson, D. Branton, J. Kasianowicz, E. Brandin, D. Deamer, 'Microsecond Time-scale Discrimination among Polycytidylic Acid, Polyadenylic Acid, and Polyuridylic Acid as Homopolymers or as Segments within Single RNA Molecules', *Biophys. J.*, **77**, 3227–3233 (1999).
14. A. Meller, L. Nivon, E. Brandin, J. Golovchenko, D. Branton, 'Rapid Nanopore Discrimination between Single Polynucleotide Molecules', *Proc. Natl. Acad. Sci. U.S.A.*, **97**, 1079–1084 (2000).
15. A. Meller, L. Nivon, D. Branton, 'Voltage-Driven DNA Translocations through a Nanopore', *Phys. Rev. Lett.*, **86**, 3435–3438 (2001).
16. J.J. Kasianowicz, M.S.Z. Kellermayer, D.W. Dreamer, eds., *Structure and Dynamics of Confined Polymers* Kluwer, Dordrecht, 2002.
17. A. Meller, 'Dynamics of polynucleotide Transport through Nanometre-scale Pores', *J. Phys.: Condens. Matter*, **15**, R581–R607 (2003).
18. M. Bates, M. Burns, A. Meller, 'Dynamics of Single DNA Molecules Actively Controlled Inside a Membrane Channel', *Biophys. J.*, **84**(4), 2366–2372 (2003).
19. J. Mathé, H. Visram, V. Viasnoff, Y. Rabin, A. Meller, 'Nanopore Unzipping of Individual DNA Hairpin Molecules', *Biophys. J.*, **87**(5), 3205–3212 (2004).
20. O.K. Dudko, G. Hummer, A. Szabo, 'Intrinsic Rates and Activation Free Energies from Single-molecule Pulling Experiments', *Phys. Rev. Lett.*, **96**, 108101 (2006).
21. O.K. Dudko, G. Hummer, A. Szabo, 'Theory, Analysis, and Interpretation of Single-molecule Force Spectroscopy Experiments', *Proc. Natl. Acad. Sci. U.S.A.*, **105**, 15755–15760 (2008).
22. E. Evans, 'Probing the Relation between Force-lifetime- and Chemistry in Single Molecule Bonds', *Annu. Rev. Biophys. Biomol. Struct.*, **30**, 105–128 (2001).
23. G.I. Bell, 'Models of the Specific Adhesion of Cells to Cells', *Science*, **200**, 618–627 (1978).
24. G. Hummer, A. Szabo, 'Kinetics from Nonequilibrium Single-molecule Pulling Experiments', *Biophys. J.*, **85**, 5–15 (2003).
25. O.K. Dudko, A.E. Filippov, J. Klafter, M. Urbakh, 'Beyond the Conventional Description of Dynamic Force Spectroscopy of Adhesion Bonds', *Proc. Natl. Acad. Sci. U.S.A.*, **100**, 11378–11381 (2003).
26. H.A. Kramers, 'Brownian Motion in a Field of Force and the Diffusion Model of Chemical Reactions', *Physica*, **7**, 284–304 (1940).
27. P. Hänggi, P. Talkner, M. Borkovec, 'Reaction-rate Theory: Fifty Years after Kramers', *Rev. Mod. Phys.*, **62**(2), 251–342 (1990).
28. O.K. Dudko, J. Mathé, A. Szabo, A. Meller, G. Hummer, 'Extracting Kinetics from Single-molecule Force Spectroscopy: Nanopore Unzipping of DNA Hairpins', *Biophys. J.*, **92**(12), 4188–4195 (2007).
29. L. Song, M.R. Hobaugh, C. Shustak, S. Cheley, H. Bayley, J.E. Gouax, 'Structure of Staphylococcal a-Hemolysin a Heptameric Transmembrane Pore', *Science*, **274**, 1859–1865 (1996).
30. X.F. Kang, S. Cheley, X.Y. Guan, H. Bayley, 'Stochastic Detection of Enantiomers', *J. Am. Chem. Soc.*, **128**(33), 10684–10685 (2006).
31. D. Jan Bonthuis, J. Zhang, B. Hornblower, J. Mathé, B.I. Shklovskii, A. Meller, 'Self-Energy-Limited Ion Transport in Subnanometer Channels', *Phys. Rev. Lett.*, **97**, 128104 (2006).
32. A.F. Sauer-Budge, J.A. Nyamwanda, D.K. Lubensky, D. Branton, 'Unzipping Kinetics of Double-stranded DNA in a Nanopore', *Phys. Rev. Lett.*, **90**(23), 238101 (2003).
33. S.E. Henrickson, M. Misakian, B. Robertson, J.J. Kasianowicz, 'Driven DNA Transport into an Asymmetric Nanometer Scale Pore', *Phys. Rev. Lett.*, **85**, 3057–3060 (2000).
34. A. Meller, D. Branton, 'Single Molecule Measurements of DNA Transport through a Nanopore', *Electrophores*, **23**, 2583–2591 (2002).
35. J. Mathé, A. Arinstein, Y. Rabin, A. Meller, 'Equilibrium and Irreversible Unzipping of DNA in a Nanopore', *Europhys. Lett.*, **73**(1), 128–134 (2006).
36. B. Hornblower, A. Coombs, R.D. Whitaker, A. Kolomeisky, S.J. Picone, A. Meller, M. Akeson, 'Single-molecule Analysis of DNA-protein Complexes using Nanopores', *Nature Methods*, **4**(4), 315–317 (2007).
37. J. Li, D. Stein, C. McMullan, D. Branton, M.J. Aziz, J.A. Golovchenko, 'Ion-beam Sculpting at Nanometre Length Scales', *Nature*, **412**, 166–169 (2001).
38. A.J. Storm, J.H. Chen, X.S. Ling, H.W. Zandbergen, C. Dekker, 'Fabrication of Solid-state Nanopores with Single-nanometre Precision', *Nat. Mater.*, **2**(8), 537–540 (2003).
39. C. Dekker, 'Solid-state Nanopores', *Nat. Nanotechnol.*, **2**(4), 209–215 (2007).
40. M.-J. Kim, M. Wanunu, C.D. Bell, A. Meller, 'Rapid Fabrication of Uniform Size Nanopores and Nanopore

Arrays for Parallel DNA Analysis', *Adv. Mater.*, **18**, 3149–3153(2006).

41. J.B. Heng, C. Ho, T. Kim, R. Timp, A. Aksimentiev, Y.V. Grinkova, S. Sligar, K. Schulten, G. Timp, 'Sizing DNA using a Nanometer-diameter Pore', *Biophys. J.*, **87**(4), 2905–2911 (2004).
42. A.J. Storm, J.H. Chen, H.W. Zandbergen, C. Dekker, 'Translocation of Double-strand DNA Through a Silicon Oxide Nanopore', *Phys. Rev. E.*, **71**, 051903-1-10 (2005).
43. D. Fologea, M. Gershow, B. Ledden, D.S. McNabb, J.A. Golovchenko, J.L. Li, 'Detecting Single Stranded DNA with a Solid State Nanopore', *Nano Lett.*, **5**(10), 1905–1909 (2005).
44. M. Gershow, J.A. Golovchenko, 'Recapturing and Trapping Single Molecules with a Solid-state Nanopore', *Nature Nanotechnol.*, **2**(12), 775–779 (2007).
45. B. McNally, M. Wanunu,, A. Meller, 'Electro-mechanical Unzipping of Individual DNA Molecules using Synthetic sub-2 nm Pores', *Nano Lett.*, **8**(10), 3418–3422 (2008).
46. M. Wanunu, J. Sutin, B. McNally, A. Chow, A. Meller, 'DNA Translocation Governed by Interactions with Solid State Nanopores', *Biophys. J.*, **95**(10), 4716–4725 (2008).